

# Antiferromagnetic triangular Blume-Capel model with hard core exclusions

A. Ibenskas,<sup>1</sup> M. Šimėnas,<sup>1</sup> and E. E. Tornau<sup>1</sup>

*Semiconductor Physics Institute, Center for Physical Sciences and Technology, Goštauto 11, LT-01108 Vilnius, Lithuania.*

(Dated: 28 February 2018)

Using Monte Carlo simulation we analyze phase transitions of two antiferromagnetic (AFM) triangular Blume-Capel (BC) models with AFM interactions between third nearest neighbors. One model has hard core exclusions between the nearest neighbor (1NN) particles (3NN1 model) and the other - between 1NN and next-nearest-neighbor particles (3NN12 model). Finite-size scaling analysis reveals that in these models, as in the 1NN AFM BC model, the transition from paramagnetic to long-range order (LRO) AFM phase is either of the first-order or goes through intermediate phase which might be attributed to Berezinskii-Kosterlitz-Thouless (BKT) type. We demonstrate that properties of the low-temperature phase transition to the AFM phase of 1NN, 3NN1 and 3NN12 models are very similar in all interval of a normalized single-ion anisotropy parameter,  $\delta$ , except for those values of  $\delta$ , where the first order phase transitions occur. Due to different entropy of the 3NN12 and 3NN1 models, their higher temperature behavior is rather different from that of the 1NN model. Three phase transitions are observed for 3NN12 model: (i) from paramagnetic phase to the phase with domains of the LRO AFM phase at  $T_c$ ; (ii) from this structure to diluted frustrated BKT-type phase at  $T_2$  (high-temperature limit of the critical line of the BKT-type phase transitions) and (iii) from this frustrated phase to the AFM LRO phase at  $T_1$  (low-temperature limit of this line). For the 3NN12 model  $T_c > T_2 > T_1$  at  $0 < \delta < 1.15$  (range I),  $T_c = T_2 > T_1$  at  $1.15 < \delta < 1.3$  (range II) and  $T_c = T_2 = T_1$  at  $1.3 < \delta < 1.5$  (range III). For 3NN1 model  $T_c = T_2 > T_1$  at  $0 < \delta < 1.2$  (range II) and  $T_c = T_2 = T_1$  at  $1.2 < \delta < 1.5$  (range III). In range III there is only one first order phase transition. In range II the transition at  $T_c = T_2$  is of the first order, too. In range I the transition at  $T_c$  is either weak first-order or second-order phase transition.

PACS numbers: 64.60.an; 64.60.De; 64.60.Ht

## I. INTRODUCTION

The self-assembly of large triangular molecules attracts nowadays a great deal of attention (see e.g. reviews<sup>1,2</sup>). The trimesic acid (TMA)<sup>3-8</sup>, BTB<sup>9,10</sup> and some other molecules<sup>11-15</sup> create patterns of different complexity on solid-liquid interface or high-quality graphite and metal surfaces in ultra vacuum conditions. The assemblies of such molecules might be different, but the, so-called, honeycomb phase is the dominating low temperature pattern.

For description of the ordering of such (or similar) molecules the statistical models of phase transitions might be used. The honeycomb phase might be understood then as the low-temperature long-range order (LRO) phase on a tripartite lattice in which the sites of each sublattice are occupied by occupation variables  $+1$ ,  $-1$  and  $0$ , respectively. For example, the ordering of triangular TMA molecules might be described by the antiferromagnetic (AFM) nearest neighbor (1NN) 3-state model<sup>16</sup> which was originally created to describe the ordering of lattice fluids and is sometimes called Bell-Lavis model<sup>17,18</sup>. This model is similar to a better known triangular AFM lattice models: Blume-Capel (BC) model<sup>19,20</sup> with some neglected interactions, Blume-Emery-Griffiths model<sup>21</sup> with anisotropic term<sup>22,23</sup> and diluted triangular AFM Ising (TAFI) model<sup>24</sup>. The ordering of large molecules requires accounting for a finite size of the ordering objects, therefore some modifications related to

hard core exclusions have to be introduced. To describe the ordering of TMA molecules into a series of flower phases, a model<sup>25</sup> with such exclusion at 1NN was proposed. In this model the initial lattice is rescaled, and the molecular interactions, which mimic the H-bonds, act between the molecules being on third nearest neighbor (3NN) sites, while the exclusion mimic the hard core infinite repulsive interaction occurring due to finite size of the molecules.

At least two important questions arise when triangular AFM and other lattice models are used (see e.g.<sup>12,13,26-29</sup>) to describe the molecular ordering: to what extent the standard models might be rescaled and what effect the exclusion brings in comparison with classical (i.e. usually 1NN) statistical models. Intuitively, it is clear that the rescaling to the  $n$ NN models (with  $n > 1$ ) changes the entropy of the system repressing the ordered phases and decreasing the phase transition temperature if more sites for molecular diffusion occur. On the other hand, the exclusion, which necessarily comes due to large size of the molecules, decreases the number of sites for diffusion and, while promoting the ordered phases, increases the transition temperature.

Here we try to answer these questions using a triangular AFM BC model with exclusions as an example. This model is tightly related to TAFI model which was extensively studied<sup>24</sup> due to its frustrated phase and large entropy at  $T = 0$ . The TAFI model with magnetic field (chemical potential) gives rise to ordered 3-

sublattice structure, denoted as  $\sqrt{3} \times \sqrt{3}$ , in which magnetizations (densities) of two sublattices are mutually equal but different from that of the third<sup>30</sup>. When diluted by the vacancies, which are not fixed, but evolve together with the spins (the, so-called, annealed vacancies), the TAFI model also allows for the 3-sublattice LRO structure. Simple substitution of occupation variables<sup>31</sup> transforms a diluted TAFI model in a field to Ising spin-1 or BC model<sup>19</sup>. The TAFI model also can be mapped into 6-state AFM clock model<sup>32</sup>. As shown by Cardy<sup>33</sup>, the 6-state clock model can exhibit either a first-order transition, two Berezinskii-Kosterlitz-Thouless (BKT) type transitions or successive Ising, three-state Potts, or Ashkin-Teller-like transitions. With decrease of temperature the 6-state AFM clock model on triangular lattice gives a succession of two very close phase transitions which are attributed to Ising (chiral) and BKT-type respectively<sup>34,35</sup>.

The earliest study<sup>20</sup> of triangular AFM BC model performed by renormalization group methods demonstrated that the AFM LRO phase, which has the sites of its three sublattices occupied by variables 1, -1 and 0 respectively, can be obtained on a phase diagram of this model. This phase occurs when the ratio of a single ion anisotropy parameter normalized to antiferromagnetic coupling,  $\delta = \Delta/|J|$ , is within limits 0 and  $3/2$ . When  $\delta > 3/2$  the gas (disordered) phase prevails. It was shown in Ref.<sup>20</sup> that the phase transitions to the LRO phase are of the second order for all  $\delta > 0$ , except at the very limit of the LRO phase,  $\delta \rightarrow 3/2$ , where the first order phase transition was found. Overstepping other limit of the LRO phase, i. e. at  $\delta < 0$ , the frustrated phase typical to the TAFI model occurs. It should be noted that treating the model spin variables as particle variables and using the lattice-gas rather than the magnetic formalism, the single ion anisotropy parameter  $\delta$  might be understood as a chemical potential. Then decrease of  $\delta$  is associated with increase of particle concentration at expense of vacancies and transition from the 3-state AFM BC model to the 2-state TAFI model (no vacancies) at  $\delta = 0$ .

Recently, a consistent study of phase transitions of this model was performed using Monte Carlo (MC) calculations<sup>36</sup>. It was clearly shown that the phase transition from the paramagnetic to the AFM LRO phase is mediated by the BKT-type phase in all interval of  $\delta > 0$  values, where the LRO AFM phase exists, except for  $\delta \gtrsim 1.47$ , where the first order phase transition between paramagnetic and LRO AFM phases is found.

In this paper we study the AFM BC model with exclusions. The problem is solved assuming the AFM interaction of spins residing on 3NN sites. Two models with hard core exclusions are considered: the 3NN model with exclusions at the 1NN sites (3NN1) and the 3NN model with 1NN and 2NN exclusions (3NN12) (see Fig. 1). It should be noted that 3NN AFM BC model without exclusions is not studied here, because it gives entirely different type of LRO AFM phase as its ground state

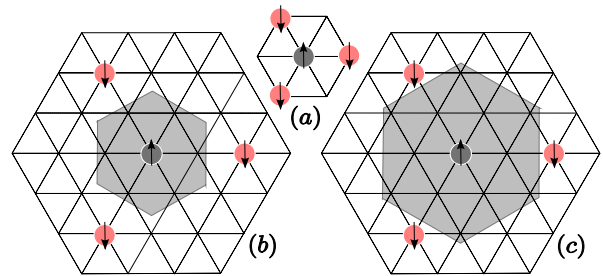


FIG. 1. (color online) Particle (spin) arrangement in the LRO AFM phase on triangular lattice for (a) 1NN, (b) 3NN1 and (c) 3NN12 models. Gray regions schematically mark the limits of interaction exclusion (infinite repulsion) for the central spin.

structure.

The obtained results for 3NN1 and 3NN12 models are compared with the results of the 1NN model. We study how the exclusion affects the type of phase transition, critical line of the BKT points and phase diagram. We demonstrate that in both 3NN models with exclusion the BKT-type phase transitions obtained in 1NN model survive. Nevertheless, the phase transitions in the 3NN1 and 3NN12 models are similar to those of the 1NN model only at lower temperature, where the transition from the BKT-type phase to the LRO AFM phase is found, and at those values of a single-ion anisotropy parameter which are not close to the gas phase limit. At higher temperature and close to this limit the properties are rather different. The exclusions decrease the high-temperature point of the BKT-type phase transition and might stimulate the occurrence of a phase transition from paramagnetic phase to the phase with domains of the LRO AFM phase. It is demonstrated in the last section of the paper that the higher temperature part of the phase diagrams of both 3NN models is very different from that of the 1NN model.

## II. MODEL AND DETAILS OF SIMULATION

The model Hamiltonian has the form

$$\mathcal{H} = -J \sum_{i,j} s_i s_j + \Delta \sum_i s_i^2, \quad (1)$$

where  $s_i = \pm 1, 0$  is the spin variable on the triangular lattice site  $i$ ,  $J$  is the antiferromagnetic ( $J < 0$ ) interaction parameter acting between the particles at 3NN sites, and  $\Delta$  is a single-ion anisotropy parameter. Here we regard the introduced variables as describing the magnetic particles in the diluted lattice-gas model rather than the spin projections. Therefore in (1) we write  $\Delta$  with plus sign and treat this parameter as a chemical potential, i.e. the total concentration of  $\pm 1$  particles increases (decreases) with decrease (increase) of  $\Delta$ . Consequently, in

the 3NN12 model the interactions between particles separated by 1NN and 2NN distances are forbidden by taking infinite repulsion of particles at these sites. In the 3NN1 model the interactions between particles in the 1NN sites are forbidden in the same way. Further, the temperature and single-ion anisotropy parameter are both normalized to  $|J|$ :  $k_B T/|J|$  and  $\delta = \Delta/|J|$ .

Since cluster algorithms for frustrated systems are known to be ineffective<sup>37</sup>, we performed the simulation of phase transition properties using local update (single-flip) Metropolis algorithm and Glauber dynamics. In the beginning the sites of a triangular lattice were randomly populated by particles in states  $+1$ ,  $1$  and  $0$ , and the initial energy  $E_i$  of a randomly chosen molecule was calculated. Then the initial state of that molecule was changed (with equal probability) to one of two remaining states, and the final energy  $E_f$  was calculated. The new state was accepted, if the energy decreased after the change of state, or accepted with the probability  $\sim \exp[-(E_f - E_i)/k_B T]$ , if increased. Thus, the calculations were performed with fixed chemical potential, while the concentration of particles in non-zero state,  $c = \sum_i s_i^2/L^2$ , was allowed to vary.

For thermal averaging MC calculations and finite size scaling (FSS) of both 3NN models with exclusions we used the triangular lattices of sizes  $L \times L$  with  $L$  from 96 up to 216. For calculations of the 1NN model, which we performed to compare the results, the lattice sizes  $L = 48, 72, 96, 120$  were used (for 1NN model  $J$  in (1) is acting between the particles on the 1NN sites). We used periodic boundary conditions and  $(0.2-1) \times 10^6$  MC steps (MCS) for thermalization. Further, we collected averages of  $10^7$  MCS for the 3NN models and  $10^6-10^7$  MCS for the 1NN model. Our simulations were performed starting from higher temperature and using random initial particle configuration. Then the temperature was gradually decreased in small steps with simulations at new temperature starting from the final configuration of the previous temperature.

Since phase transition parameters in this system were often characterized by abruptness of their thermodynamic parameters and first order phase transitions, in particular, we performed also energy histogram calculations using reweighting techniques<sup>38</sup>. For these calculations we used slightly larger lattice sizes ( $L = 120 - 270$ ) than for the thermal averaging. In some cases we used a very large lattice size,  $L = 360$  and  $399$ . Our simulations of thermodynamic parameters (energy derivatives) often proceeded as follows: the phase transition point was located by thermal averaging and then its slight correction was performed by reweighting calculations.

We also performed the analysis of the autocorrelation time of energy at  $T_c$  at  $\delta = 0.7$  for both 3NN models. The integrated autocorrelation time for the 3NN12 model ranged from  $\tau \sim 10^3$  MCS for  $L = 120$  to  $\tau \sim 10^5$  MCS for  $L = 399$ . For the 3NN1 model this time is around one-two orders of magnitude higher.

For studies of phase transitions we used the AFM or-

der parameter. It should be noted, that low temperature AFM phase of the 1NN model is stabilized when each sublattice of the tripartite lattice is occupied by  $+1$ ,  $-1$  and  $0$  variables, respectively. The distance between so-occupied sites is one lattice constant of a triangular lattice,  $a$ . The stoichiometric particle concentration (coverage of sites occupied by the  $\pm 1$  particles) in the 1NN model is  $c_s = 2/3$ . Low temperature AFM phase of both 3NN models has 12 sublattices, only two of which are occupied by the  $+1$  and  $-1$  particles, respectively, and all other sublattices are empty. Therefore the distance between  $+1$  and  $-1$  particles is  $2a$  and  $c_s = 1/6$  in the AFM phase of both 3NN models. As an order parameter, we use the staggered magnetization, a slightly reworked version of the one suggested for the 1NN model<sup>36</sup>. It is the average difference of maximally and minimally occupied sublattices. For 3NN model we had to account for occupancy of 12 sublattices, and therefore the staggered magnetization has the form

$$m_s = \langle M_s \rangle / L^2 = 6 \left\langle \max \left( \sum_{i1 \in \text{sub1}} s_{i1}, \sum_{i2 \in \text{sub2}} s_{i2}, \dots, \sum_{i12 \in \text{sub12}} s_{i12} \right) - \min \left( \sum_{i1 \in \text{sub1}} s_i, \sum_{i2 \in \text{sub2}} s_{i2}, \dots, \sum_{i12 \in \text{sub12}} s_{i12} \right) \right\rangle / L^2. \quad (2)$$

Here  $i1 \dots i12$  denote sites belonging to each sublattice, and the factor 6 is needed to compensate for the stoichiometric concentration of the AFM phase in the 3NN models. We calculate also temperature dependences of the specific heat  $C_v = (\langle \mathcal{H}^2 \rangle - \langle \mathcal{H} \rangle^2) / L^2 k_B T^2$ , susceptibility  $\chi = (\langle M_s^2 \rangle - \langle M_s \rangle^2) / L^2 k_B T$ , logarithmic derivatives of  $\langle M_s \rangle$  and  $\langle M_s^2 \rangle$

$$D_{1s} = \frac{\partial \ln \langle M_s \rangle}{\partial \beta} = \frac{\langle M_s \mathcal{H} \rangle}{\langle M_s \rangle} - \langle \mathcal{H} \rangle \quad (3)$$

$$D_{2s} = \frac{\partial \ln \langle M_s^2 \rangle}{\partial \beta} = \frac{\langle M_s^2 \mathcal{H} \rangle}{\langle M_s^2 \rangle} - \langle \mathcal{H} \rangle$$

and Binder order parameter and energy cumulants,  $U_B^m = 1 - \langle M_s^4 \rangle / 3 \langle M_s^2 \rangle^2$  and  $U_B^E = 1 - \langle \mathcal{H}^4 \rangle / 3 \langle \mathcal{H}^2 \rangle^2$ , respectively. The functions  $D_{1s}$  and  $D_{2s}$  were introduced in Ref.<sup>39</sup>. They were shown<sup>36</sup> to be useful for a finite-size scaling of the 1NN AFM BC model. At the second order phase transition point  $T_c$  the maximum of specific heat and susceptibility scale as  $C_v \sim L^{\alpha/\nu}$  and  $\chi \sim L^{\gamma/\nu}$ , respectively, while minimum of  $D_{1s}$  and  $D_{2s}$  - as  $\sim L^{1/\nu}$ . Here  $\alpha$ ,  $\beta$  and  $\nu$  are critical exponents of specific heat, susceptibility and correlation length, respectively. At the first order phase transition at  $T_c$  the extrema of all these functions scale as  $\sim L^{d/40}$ , where  $d$  is dimensionality of the system.

In a following section we present the values of critical exponent ratios  $\alpha/\nu$  and  $1/\nu$  at the phase transition point from the paramagnetic phase,  $T_c$ . The ratio  $\alpha/\nu$  is obtained either by combined thermal averaging and

reweighted histogram calculation of specific heat maximum at  $T_c$  or by scaling these values close to  $T_c$  and using the formula  $C_v - C_0 \sim L^{\alpha/\nu} f(tL^{1/\nu})$  (here  $t = |T_c - T|/T_c$  and background is assumed to be  $C_0 = 0$ ). The latter formula also gives the value of  $1/\nu$  which we alternatively obtain as the average of scaling of parameters  $D_{1s}$  and  $D_{2s}$ .

In a case of BKT-type phase transitions correlation length diverges as  $\xi = \xi_0 \exp\{a[(T_{\text{BKT}} - T)/T_{\text{BKT}}]^{-1/2}\}$  and spin-correlation function decays as  $\langle s_i s_j \rangle \sim r_{ij}^{-\eta}$ , where  $\eta$  is the critical exponent of the correlation function<sup>41</sup>. The order parameter at the BKT-type of phase transition point scales as  $m_s(L) \sim L^{-\eta/2}$ . The exponent  $\eta$  might also be obtained from a part of susceptibility  $\chi' = \langle M_s^2 \rangle / L^2 k_B T \sim L^{2-\eta}$ <sup>42</sup>. To obtain accurate values of the BKT-type phase transitions of the AFM BC 1NN model at  $T_1$  and  $T_2$ , the FSS of parameters  $m_s$  and  $\chi'$  was performed<sup>36</sup>. The following relations were used

$$m_s L^b = f_1 \left\{ L^{-1} \exp \left[ a \left( \frac{T_1 - T}{T_1} \right)^{-1/2} \right] \right\}, \quad T < T_1 \quad (4)$$

$$\chi' L^c = f_2 \left\{ L^{-1} \exp \left[ a \left( \frac{T - T_2}{T_2} \right)^{-1/2} \right] \right\}, \quad T > T_2$$

where  $b = \eta/2$  and  $c = 2 - \eta$  and  $T_1$  and  $T_2$  are lower-temperature AFM LRO phase – frustrated (BKT-type) phase and higher-temperature frustrated phase – paramagnetic phase transition temperatures, respectively.

### III. RESULTS OF SIMULATION

Both 3NN12 and 3NN1 models, as well as the 1NN model, have the low-temperature AFM phase at values of the single-ion anisotropy parameter  $\delta$  in between 0 and  $3/2$ . The behaviour and properties of phase transitions are different for different values of  $\delta$ . For the 3NN12 model we found three important ranges of  $\delta$  values. The range I corresponds to the situation when there are three consecutive phase transitions: two of them are of the BKT-type ( $T_1$  and  $T_2$ ), and they frame the critical line of the BKT-type phase transitions, and the third is a high-temperature phase transition at  $T_c$ . In range II there remains the critical line of the BKT-type phase transition points, and  $T_1$  as its low-temperature point, but  $T_2 = T_c$ . This range is found for both 3NN12 and 3NN1 models. In range III there is just one first order phase transition at  $T_1 = T_2 = T_c$ . This range is found for both 3NN12 and 3NN1 models (as well as for the 1NN model at  $\delta > 1.47$ ; in between 0 and 1.47 the 1NN model demonstrates just two BKT-type phase transitions at  $T_1$  and  $T_2$ <sup>36</sup>).

#### A. 3NN12 model at $\delta = 0.7$ (range I)

The attraction of different particles at the 3NN sites and exclusion rules imposed on 1NN and 2NN neighbors

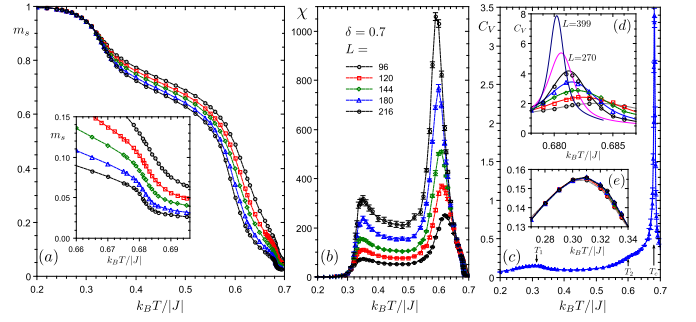


FIG. 2. (Color online) Temperature dependence of (a) staggered magnetization and (b) susceptibility of the 3NN12 model at  $\delta = 0.7$  for different values of  $L$ . Inset in (a): magnified behavior of  $m_s(T)$  at  $T_c$ . Errors in (a) do not exceed symbol size. (c) Temperature dependence of specific heat of the 3NN12 model at  $\delta = 0.7$  and  $L = 180$ . Insets in (c) show  $C_v(T)$  dependence around  $T_c$  (d) and  $T_1$  (e) for different values of  $L$ . The symbols and solid lines in (d) denote the results of thermal averaging and reweighting, respectively.

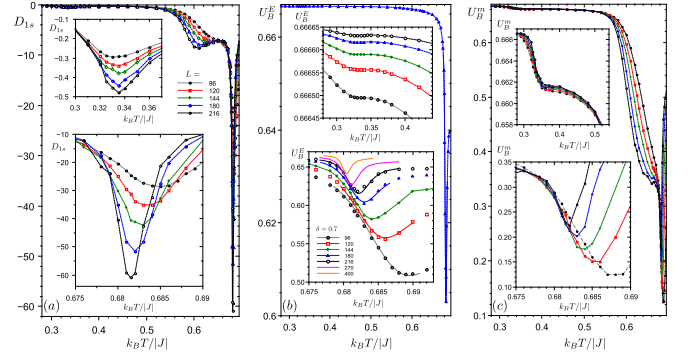


FIG. 3. (Color online) Temperature dependence of (a) parameter  $D_{1s}$  and Binder cumulants  $U_B^E$  (b) and  $U_B^m$  (c) of the 3NN12 model at  $\delta = 0.7$  and different values of  $L$ . Magnified dependences close to transitions at  $T_1$  and  $T_c$  are shown in upper and lower insets, respectively. Symbols correspond to thermal averaging results, dashed lines are guides to the eye. In lower inset of (b) the results of histograms reweighting close to  $T_c$  are shown by solid lines.

makes the 3NN12 model similar (just scaled-out) version of the 1NN model. This is indeed the case at low temperature. The situation at higher temperature is rather different.

Temperature dependence of staggered magnetization (Fig. 2a) demonstrates that 3NN12 model has three phase transitions at  $\delta = 0.7$ . In addition to two transitions at  $T_1$  and  $T_2$  (which correspond to peaks of susceptibility in Fig. 2b), the high temperature phase transition at  $T_c$  is nicely visible as a twist of  $m_s(T)$  dependence at very low values of  $m_s < 0.05$ . In temperature dependence of susceptibility, the  $T_c$  might be noticed as a small higher-temperature shoulder of the peak at  $T_2$ . However, the transition at  $T_c$  corresponds to the main high-temperature peak in the  $C_v(T)$  dependence (Fig. 2c, d), and here the transition at  $T_2$  is its hardly dis-

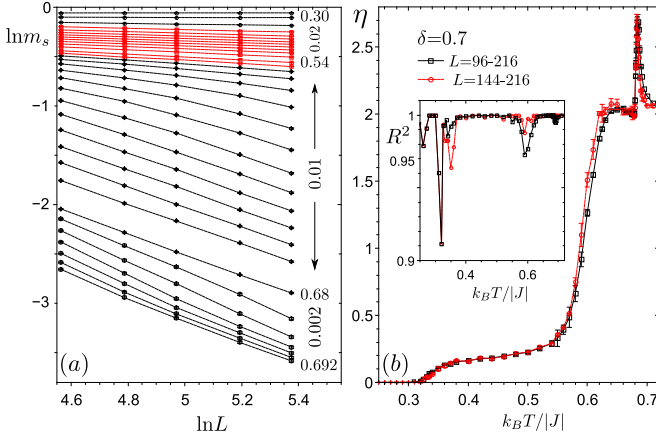


FIG. 4. (Color online) (a) Log-log plot of  $m_s$  vs  $L$  for 3NN12 model at  $\delta = 0.7$  in a temperature interval comprising the phase transition points at  $T_1$ ,  $T_2$  and  $T_c$ . The BKT-type transition region is shown by red lines. (b) Temperature dependence of parameter  $\eta$  calculated for 5 (black curve) and 3 largest (red curve) lattice sizes. Inset: temperature dependence of a linear fit accuracy parameter  $R^2$  for both cases.

cernible lower-temperature satellite (Fig. 2c). The transition at  $T_1$  is very weakly  $L$ -dependent (Fig. 2e).

All three transitions are best manifested (see Fig. 3a) in temperature dependences of parameters  $D_{1s}$  and  $D_{2s}$  (3) which combine the contributions of energy and order parameter. The Binder cumulants of energy and magnetization are shown in Figs. 3b and c. In both of them the transition at  $T_1$  is manifested as a smooth continuous step and the transition at  $T_c$  - as a deep minimum. The transition at  $T_2$  is not seen in  $U_B^E$ , but clearly seen in  $U_B^m$  in between the transitions at  $T_1$  and  $T_c$ .

Visually, the  $m_s(T)$  dependence between the transition points at  $T_1$  and  $T_2$  suggests similarity of this dependence to the 1NN model. Analysis of log-log plots of magnetization vs  $L$  (Fig. 4a) corroborates the finding of the 1NN model that the transitions at  $T_1$  and  $T_2$  belong to the BKT-type phase transitions. This is seen from the temperature dependence of the critical exponent of the correlation function,  $\eta$  (Fig. 4c), which for the BKT-type transitions should correspond to the doubled slope of lines in Fig. 4a. In temperature range between 0.35 and 0.55 the parameter  $\eta$  clearly demonstrates a plateau. The interval of  $\eta$  values in the plateau roughly coincides with classical predictions for the critical line of the BKT-type phase transitions<sup>43</sup>. We performed the FSS analysis using formula (4) to obtain more accurate values of transition temperatures  $T_1$  and  $T_2$  and  $\eta$ . The results are shown in Fig. 5a and b. The best fit was obtained for the values  $k_B T_1/|J| = 0.35 \pm 0.01$ ,  $\eta(T_1) = 0.12 \pm 0.02$  and  $k_B T_2/|J| = 0.55 \pm 0.01$ ,  $\eta(T_2) = 0.29 \pm 0.02$ . As for the 1NN model, the obtained value of  $T_1$  is a bit higher than that at the peak of  $C_v$  and very similar to that at the peak of  $\chi$ , while  $T_2$  lies lower than that obtained at the peak of  $\chi$ . It should be also noted, that we expected some error in determination of the  $T_2$  point, since

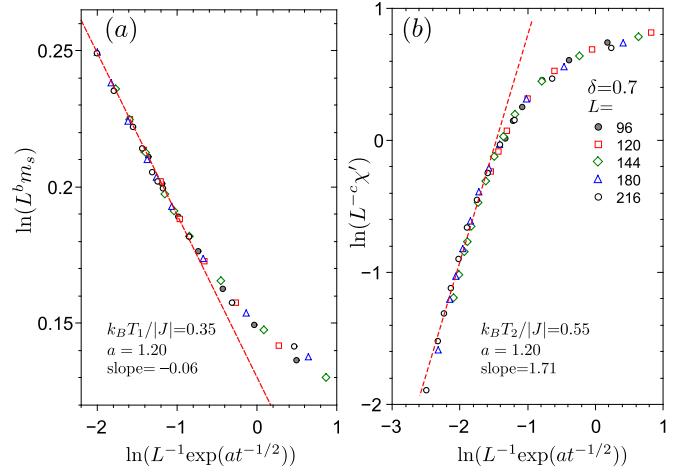


FIG. 5. (Color online) Finite-size scaling of (a)  $m_s$  at  $T_1$  ( $t = (T_1 - T)/T_1$ ) and (b)  $\chi'$  at  $T_2$  ( $t = (T - T_2)/T_2$ ) for 3NN12 model at  $\delta = 0.7$  obtained using first and second scaling relations (4), respectively.

in the 3NN12 model, differently from the 1NN model, the transition at  $T_2$  is not from the paramagnetic phase, but from the structure existing between  $T_2$  and  $T_c$  (see below). Still, as might be seen from Fig. 5b the scaling is quite satisfactory.

The  $\eta$  interval of the BKT points is rather close to the one obtained in similar models: the 1NN model (0.12-0.29)<sup>36</sup>, the planar rotator model with sixfold symmetry breaking fields  $(1/9-1/4)$ <sup>43</sup>, 6-state AFM clock model  $((0.13-0.25)$ <sup>35</sup> and  $(0.1-0.275)$ <sup>42</sup>) and TAFI model with 2NN ferromagnetic interactions  $(0.15-0.27)$ <sup>44</sup>.

The calculation of the Binder magnetic fourth-order cumulant  $U_B^m$  also demonstrated that transitions at  $T_1$  and  $T_2$  belong to universality class of the BKT-type phase transitions. The  $U_B^m(L)$  vs  $U_B^m(L')$  plots revealed that basically  $U_B^m(L) \rightarrow U_B^m(L')$  with increase of  $L' < L$ , and consequently  $\nu \rightarrow \infty$  in the formulae,  $\partial U_B^m(L')/\partial U_B^m(L) = (L'/L)^{1/\nu}$ , as for the BKT-type phase transition point.

It should be also noted that the  $\eta(T)$  dependence (Fig. 4c) also “feels” the phase transition at  $T_c$  demonstrating a sharp peak at the same value of temperature where the extrema of  $D_{1s}$ ,  $D_{2s}$  and  $C_v$  are obtained. This is not unexpected: the point at  $T_c$  is critical. The high value of  $\eta$  at  $T_c$  makes it impossible to assign this transition to universality class of the BKT-type of transitions, raising a challenging problem of its attribution. If the phase transition would be of the second order, the order parameter at  $T_c$  should scale as  $\sim L^{-\beta/\nu}$ . However, the value of  $\beta/\nu$  is much too large and inconsistent with the second-order phase transition, the indication that the first-order phase transition might take place at  $T_c$ .

We noticed that this transition occurs at approximately same concentration of particles as the stoichiometric concentration of the low-temperature LRO AFM phase (see Fig. 6). Visual inspection of instant particle



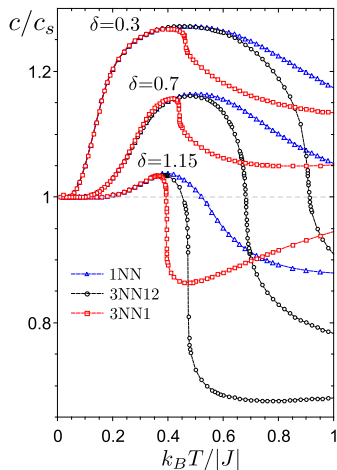


FIG. 6. (Color online) Temperature dependence of concentration for three models at  $L = 120$ : 1NN (blue triangles), 3NN12 (black squares) and 3NN1 (red squares) at  $\delta = 0.3$ , 0.7 and 1.15.

configuration reveals marked increase (in comparison to the paramagnetic phase) of hexagons with side length  $2a$  and alternation of  $+1$  and  $-1$  variables on the vertices and  $0$  in the center, i.e. hexagons typical to the low- $T$  phase of the 3NN12 model. These domains of low-temperature phase exist in a very small interval of temperature between  $T_c$  and  $T_2$ . Decrease of temperature from  $T_c$  leads to an increase of concentration which results in population of centers of mentioned hexagons and formation of a frustrated structure at  $T_2$ , the structure which further continues up to the phase transition point at  $T_1$ . This increase of concentration is rather abrupt in comparison to a smooth and continuous increase of  $c$  characteristic to the 1NN model (compare curves in Fig. 6). Thus, at  $T_c$  we obtain a strongly diluted phase with domains of the low-temperature AFM LRO phase. It is known that dilution in frustrated systems leads to phase transitions with non-classical critical exponents, broad two-maxima histograms with high saddle point, ambiguous behaviour of interface energy and, in general, makes the FSS analysis very complicated<sup>45</sup>.

The energy histograms at the  $T_c$  point and  $\delta = 0.7$  are shown in Fig. 7. They are two-peaked and remain such up to the largest lattice size studied here,  $L = 399$ . We calculated interface tension,  $2\sigma = \ln(P_{\max}(L)/P_{\min}(L))/L$ , and latent heat,  $\Delta E = |E_+ - E_-|$ , using these energy histograms. Here  $P_{\max}(L)$  and  $P_{\min}(L)$  are probability density of energy at maximum and saddle point, respectively, and  $E_+(L)$  and  $E_-(L)$  are the energies at right and left peaks of energy distribution at  $T_c$ . The  $2\sigma$  even up to  $L = 399$  depends on  $L$  - thus, we are not sure if we have reached the lattice sizes suitable for the finite size scaling, but  $L = 399$  was the limit of our computer resources. The saddle point slightly decreases with  $L$  which would indicate in favor of the first order phase transition, though the behavior is

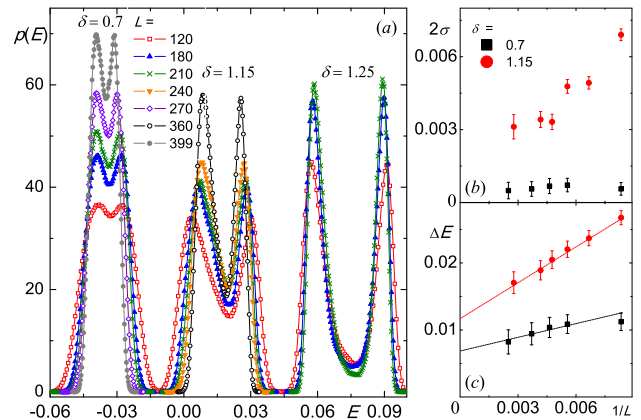


FIG. 7. (Color online) (a) Energy histograms of 3NN12 model at  $\delta = 0.7$ , 1.15 and 1.25 (the latter is shifted along energy axis by 0.05). (b) and (c) show  $L$ -dependence of interface tension and latent heat, respectively.

rather different from that of the typical first order phase transition (which will be seen in region III). If to neglect the two smallest lattice sizes, the interface tension and latent heat, decrease with increase of  $L$  as shown in insets to Fig. 7. The  $\Delta E$ , most likely, tends to a finite value.

The results of specific heat scaling close to  $T_c$  are given in Fig. 8a. At  $\delta = 0.7$  the values of critical exponent ratios  $\alpha/\nu = 1.04 \pm 0.05$  and  $1/\nu = 1.64 \pm 0.05$  are obtained. The calculation of  $\alpha/\nu$  from magnitude of  $C_v$  peak at  $T_c$  for lattice sizes  $L = 180 - 399$  yields the same result,  $\alpha/\nu = 1.04$  (see Fig. 8c). Calculation of  $1/\nu$  from minima of  $D_{1s}$  and  $D_{2s}$  at  $T_c$  for lattice sizes  $L = 144 - 216$  gave us much smaller critical exponent of the correlation length,  $1/\nu = 1.0 \pm 0.05$ .

We also performed histograms and critical exponents calculation at another point of region I,  $\delta = 0.3$ . The saddle point of these histograms is even higher than in the case  $\delta = 0.7$ , correspondingly the interface tension is a bit smaller. The latent heat is similar to that of  $\delta = 0.7$ . The scaling performed at  $\delta = 0.3$  gives the following critical exponents  $\alpha/\nu = 0.83 \pm 0.05$  (the same value as from the fitting of  $C_v(T_c)$ , see Fig. 8c) and  $1/\nu = 1.5 \pm 0.05$ . The critical exponents obtained here from scaling of  $D_{1s}$  and  $D_{2s}$  at  $T_c$  give  $1/\nu = 1.0 \pm 0.05$ , the same as for  $\delta = 0.7$ .

Thus, in range I at  $T_c$  we do not obtain standard values  $1/\nu = \alpha/\nu = d = 2$  as for the first order phase transitions. In general, the behavior of thermodynamic parameters at  $T_c$  are much smoother in range I than in ranges II and III. We assume that in the range I this transition is either a weak first order phase transition, as often encountered in models with site or bond dilution<sup>45</sup>, or a second order phase transition with the latent heat approaching to zero for such values of  $L$  which exceed considerably our computer resources (the value  $1/\nu = 1$  obtained from scaling of parameters  $D_1$  and  $D_2$

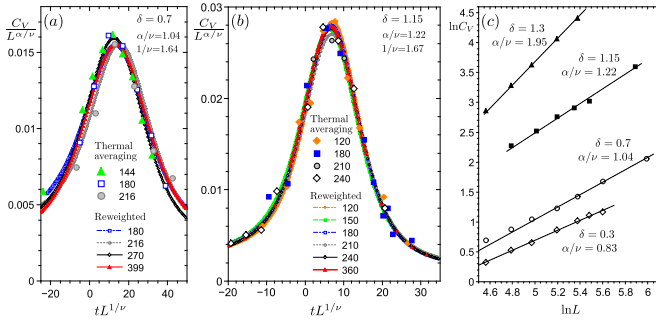


FIG. 8. (Color online) Finite-size scaling of specific heat at  $T_c$  for the 3NN12 model: (a)  $\delta = 0.7$  and (b) 1.15. The results are fitted using formula  $C_v - C_0 \sim L^{\alpha/\nu} f(tL^{1/\nu})$ , where  $t = |T_c - T|/T_c$  and background is assumed to be  $C_0 = 0$ . Large symbols correspond to the results of thermal averaging, lines and small symbols - to results obtained close to  $T_c$  by reweighted histogram method. (c) Log-log dependences of  $C_v$  maximum vs  $L$  at different values of  $\delta$ .

for  $\delta = 0.3$  and  $0.7$  is the same as for the Ising universality class). Thus, non-standard critical exponents obtained at  $T_c$  in this range might be considered as a very crude approximation only. We do not exclude the possibility that the results would probably change for considerable increase of  $L$ .

It should be noted though, that at  $\delta = 0.7$  the obtained set of critical exponents is rather close to the one obtained by Landau<sup>44</sup> for tricritical region of the TAFI model with ferromagnetic 2NN interactions ( $\alpha/\nu = 1.02$  and  $1/\nu = 1.59$ ). In comparison, the theoretical predictions for the tricritical point of the 3-state Potts model<sup>46</sup> are  $\alpha/\nu = 10/7 = 1.43$  and  $1/\nu = 12/7 = 1.71$ .

### B. 3NN12 model at other values of $\delta$ (ranges II and III)

The study of the 3NN12 model at other values of  $\delta$  allowed to determine the exact location of three ranges with different behavior of phase transitions. We found that the ranges I ( $T_c > T_2 > T_1$ ), II ( $T_c = T_2 > T_1$ ) and III ( $T_c = T_2 = T_1$ ) correspond to following ranges of  $\delta$  values: 0 - 1.15, 1.15 - 1.3 and 1.3 - 1.5, respectively. The transitions at  $T_c$  in range III is clearly of the first order. It is demonstrated by energy histograms for  $\delta = 1.3$  and 1.45 presented in Fig. 9. The saddle point in this region is much lower than in region I and decreases with increase of  $L$ . For  $\delta \approx 1.3 - 1.5$  this tendency only increases: at  $\delta = 1.45$  the peaks are separated by a huge gap (no saddle at all).

The same, just not so strong tendency to the first order phase transitions is seen in range II. We have chosen the points  $\delta = 1.15$  and  $\delta = 1.25$  for more thorough examination. The histograms at these points are presented in Fig. 7. The interface tension and latent heat are much higher than in range I. In principle, with respect to the order of transition at  $T_c$ , this range is intermediate between the ambivalent-order phase transition in range I and the

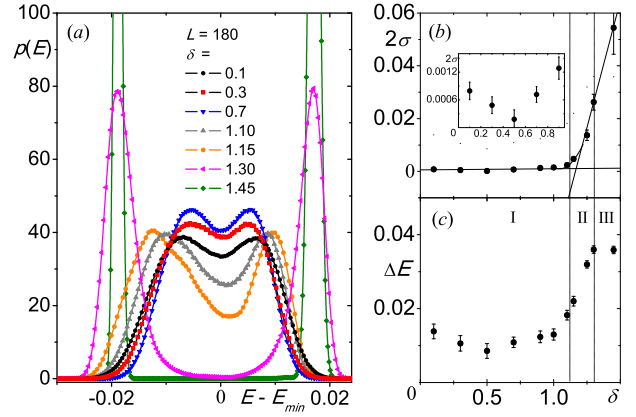


FIG. 9. (Color online) (a) Energy histograms at various values of  $\delta$  at  $T_c$  for  $L = 180$  lattice. Corresponding  $\delta$ -dependences of interface tension and latent heat are given in (b) and (c), respectively.

first-order phase transition in range III. If the transitions in range I turned out to be of the second order, the range II would be the tricritical region.

Different properties of phase transition at  $T_c$  in ranges II and III, on one hand, and I, on the other, might be seen analyzing the energy histograms (Fig. 9a) at fixed  $L$  and various values of  $\delta$ , especially  $\delta$ -dependences of interface tension  $2\sigma$  and latent heat  $\Delta E$  at  $T_c$  (Fig. 9b and c). It is seen that both these parameters clearly increase for higher values of  $\delta$ . Here we can notice the separation of the system into three mentioned ranges of behaviour: the range I featuring two-peaked histograms with high saddle point, the range III demonstrating typical first-order phase transition and the intermediate range II. In Fig. 9b the intersection of two lines corresponding to types of behavior in ranges I and III is around 1.1-1.2 for  $L = 180$ . It should be noted here that even the behavior in  $0 < \delta < 0.9$  region is not so homogeneous as might be assumed from main Fig. 9b. The detailed inset in this Fig. demonstrates that interface tension slightly increases when the limit of the TAFI model,  $\delta = 0$ , is approached and therefore has some minimum around  $\delta \approx 0.5$ , the minimum which survives also for other values of  $L$ .

Rather similar result, demonstrating the division into several ranges of behavior, is obtained analyzing the magnitude of minimum related to  $T_c$  of both Binder cumulants,  $U_B^m(T_c)$  and  $U_B^E(T_c)$ . They have two very different regions of behavior: up to approximately  $\delta = 0.9$  the minimum of  $U_B^m$  is around 0.3-0.1, but drastically decreases for higher values of  $\delta$ . The minimum of  $U_B^E$  is rather close to the  $2/3$  limit up to  $\delta = 0.7$ , but again start to rather abruptly decrease at higher values of  $\delta$ .

The results of our thermal averaging MC simulation in ranges II and III demonstrate that the thermodynamic parameters close to  $T_c$  either show thin and high extrema

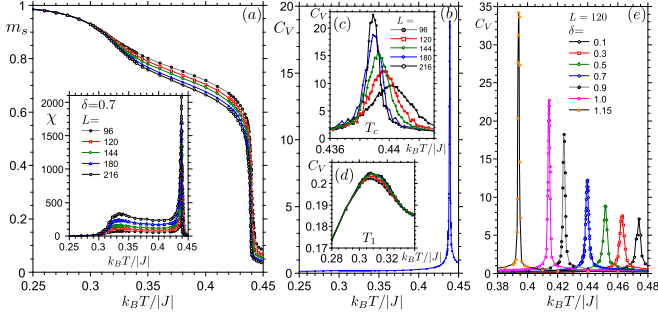


FIG. 10. (Color online) Temperature dependence of (a) staggered magnetization, (inset in (a)) susceptibility and (c, d) specific heat close to transition points  $T_2 = T_c$  and  $T_1$  of the 3NN1 model at  $\delta = 0.7$  and different values of  $L$ . (b) The  $C_v$  vs  $T$  dependence at  $\delta = 0.7$  and  $L = 120$ . (e) The  $C_v$  vs  $T$  dependence at  $L = 120$  and different values of  $\delta$ .

( $C_v$  and  $D_{1s}$ ,  $D_{2s}$ ) or abruptness similar to jump ( $m_s$  and average energy), see e.g. the behavior of normalized coverage at  $\delta = 1.15$  in Fig. 6. Thus, these results just confirm the results obtained by histogram calculations that the phase transitions in these two regions are of the first order.

In ranges II and III we also performed FSS analysis and determined the ratios of critical exponents. We obtained  $\alpha/\nu = 1.22, 1.68$  and  $1.95 (\pm 0.05)$  and  $1/\nu = 1.67, 1.94$  and  $1.99$  for  $\delta = 1.15, 1.25$  and  $1.3 (\pm 0.05)$ , respectively. Some results of this analysis are presented in Fig. 8b and c. While the values of  $\alpha/\nu$  and  $1/\nu$  at limiting points of the range II,  $\delta = 1.25$  and  $1.3$ , tend to the value 2 and are further stabilized at  $d = 2$  for  $\delta > 1.3$  (range III), the values at the other limiting point,  $\delta = 1.15$ , are closer to those of the range I (and point  $\delta = 0.7$ , in particular).

### C. 3NN1 model (ranges II and III)

In the 3NN1 model the exclusion of only 1NN sites leaves more sites for diffusion of particles, in comparison to the 1NN and 3NN12 models, correspondingly increasing the configurational entropy of the system. This does not affect the low-temperature transition point to the AFM LRO phase at  $T_1$ , but decreases the high-temperature phase transition point from the paramagnetic phase at  $T_c$ . As a result,  $T_c$  falls into the critical line of the BKT-type phase transition points and becomes inseparable from the high-temperature end of this line,  $T_2 = T_c$ , in interval of  $\delta$  values,  $0 < \delta \lesssim 1.2$  (region II). The first-order phase transition region III, where all transition points coincide,  $T_2 = T_1 = T_c$ , is at  $1.2 \lesssim \delta < 1.5$ . Thus, at  $0 < \delta \lesssim 1.2$  the behavior of the 3NN1 model at  $T_c$  is expected to be similar to that of the 3NN12 model in region II ( $1.15 < \delta < 1.3$ ). Thus, the question arises if the point at  $T_2 = T_c$  is the higher-temperature end of the BKT-type phase transitions, as in the 1NN model, or has the properties of the first-order phase transition

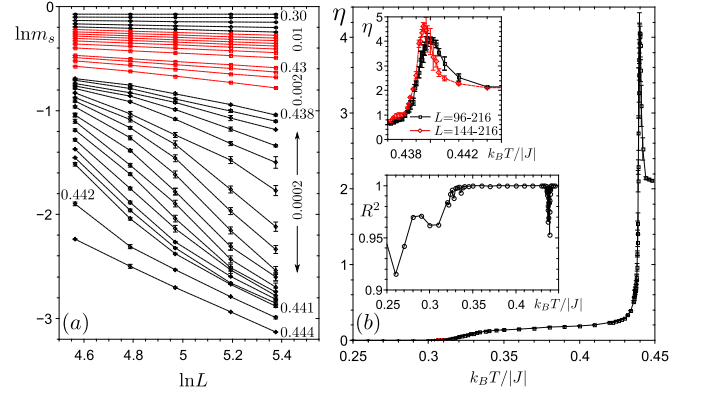


FIG. 11. (Color online) (a) Log-log plot of  $m_s$  vs  $L$  for 3NN1 model at  $\delta = 0.7$  in a temperature interval comprising the phase transition points at  $T_1$  and  $T_2 = T_c$ . The BKT-type transition region is shown by red lines. (b) Temperature dependence of parameter  $\eta$  obtained from (a). Insets: (upper)  $\eta(T)$  dependence close to  $T_c$  peak for five (black curve) and three largest (red curve) lattice sizes, respectively; (lower) temperature dependence of a linear fit accuracy parameter  $R^2$ .

as in the region II of the 3NN12 model.

The  $m_s(T)$  dependence at  $\delta = 0.7$  is given in Fig. 10a. There are no qualitative changes in comparison to the 1NN and 3NN12 models at  $T_1$ , where we can expect the low-temperature BKT-type phase transition. At  $T_2 = T_c$  the  $m_s(T)$  curve is weakly-dependent on  $L$ , which would make it a likely candidate for the BKT-type transition. On the other hand, the dependence at this point is very abrupt as in the case of the first-order phase transition. The peak of susceptibility (inset in Fig. 10a) at  $T_2 = T_c$  is much higher than that of the 3NN12 model at the  $T_2 < T_c$ , but comparable with the one obtained in the 3NN12 model when  $T_2 = T_c > T_1$  at  $1.15 < \delta < 1.3$ . Specific heat  $C_v$  demonstrates (Fig. 10b) a sharp peak at  $T_c = T_2$  which depends on  $L$  (Fig. 10c) and clearly increases with increase of  $\delta$  (Fig. 10e). The  $C_v$  also shows very small in comparison to the main peak and almost  $L$ -independent peak at  $T_1$  (Fig. 10d).

Log-log plots of  $m_s$  vs  $T$  dependence (Fig. 11a) and, consequently,  $\eta$  vs  $T$  dependence in Fig. 11b clearly demonstrate the region of the BKT-type phase transitions and  $T_1$  as its low-temperature end ( $\eta \sim 0.12$  at  $T_1$ ). However, the high-temperature end of the BKT-type transitions line shows a high peak at  $T_2 = T_c$  instead of rounding which is characteristic to  $T_2$  encountered in the 1NN and 3NN12 models. Moreover, the FSS analysis of the phase transition point close to  $T_1$  might be performed (see Fig. 12a) using the first formula (4), and the best fit gives  $T_1 = 0.34 \pm 0.01$  and  $\eta(T_1) = 0.12 \pm 0.02$ . However, the FSS analysis using second formula (4) close to  $T_c = T_2$  is rather unsuccessful. The critical behavior at the  $T_c = T_2$  peak of  $\eta(T)$  dependence is also inconsistent with any reasonable  $\beta/\nu$  values related to the second-order phase transitions. All these facts indicate that for



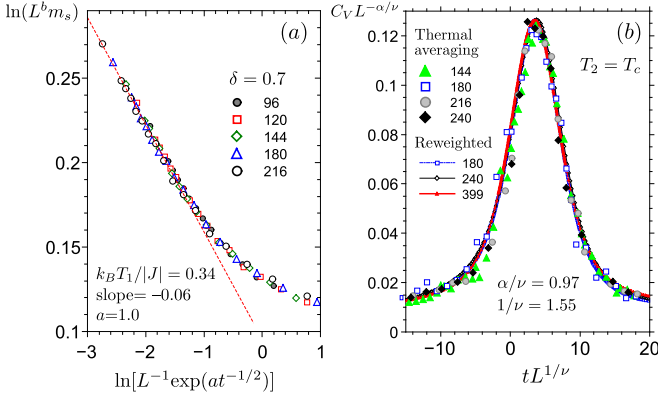


FIG. 12. (Color online) Finite-size scaling of the 3NN1 model parameters at  $\delta = 0.7$ : (a)  $m_s$  at  $T_1$  ( $t = (T_1 - T)/T_1$ ) and (b)  $C_v$  at  $T_c = T_2$  using scaling relation  $C_v \sim L^{\alpha/\nu} f(tL^{1/\nu})$ , where  $t = |T_c - T|/T_c$ .

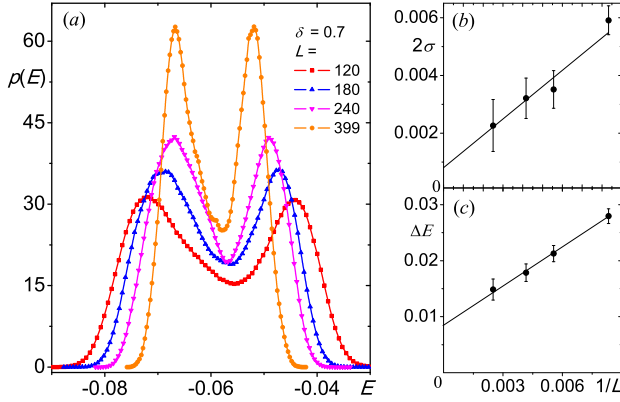


FIG. 13. (Color online) (a) Energy histograms, (b) interface tension  $2\sigma = \frac{1}{L} \ln(P_{\max}/P_{\min})$  and (c) latent heat of the 3NN1 model at  $\delta = 0.7$ .

the 3NN1 model the transition at  $T_1$  is the BKT-type phase transition, but the high-temperature transition at  $T_2 = T_c$  - is not. The latter conclusion is further confirmed by the histograms calculation. The saddle point in two-peak energy histograms of Fig. 13a at  $\delta = 0.7$  rather systematically decreases with increase of  $L$ , supporting the idea of the first-order phase transition at this point.

One more argument in favor of the first order phase transition at  $T_2 = T_c$  of the 3NN1 model in region II comes from analysis of the autocorrelation time of energy. As mentioned, the integrated autocorrelation time for the 3NN1 model at  $\delta = 0.7$  and  $T_c = T_2$  is around one-two orders of magnitude higher than for the 3NN12 model at  $\delta = 0.7$  and  $T_c > T_2$  and is approximately  $\tau \sim 10^4 - 10^5$  for  $L = 120$  and close to the limit of our calculations,  $\tau \sim 10^6 - 10^7$ , for  $L = 399$ . Such difference between the autocorrelation times for both models indicates much stronger first-order nature of the transition at  $T_2 = T_c$  of

the 3NN1 model.

Nevertheless, the extrema of  $C_v$  and  $D_{1s}, D_{2s}$  parameters in region II at  $T_2 = T_c$  do not scale with  $L^2$  as for the usual first-order phase transition. This is clearly seen extending the lattice sizes up to  $L = 399$ . The  $C_v$  scales with critical exponents  $\alpha/\nu = 0.97 \pm 0.05$  and  $1/\nu = 1.55 \pm 0.05$  (Fig. 12b). The FSS of  $D_{1s}$  and  $D_{2s}$  parameters gives very similar result for  $1/\nu$ . The same is true when  $1/\nu$  is obtained from scaling of  $T_c(L) = T_c(\infty) + aL^{-1/\nu}$ , when  $T_c(\infty)$  is the one used for scaling in Fig. 12b.

The first-order type of transition at  $\delta > 1.2$  (region III) is much more explicit than at  $\delta = 0.7$ . The critical exponents tend to 2 demonstrating typical first-order behaviour at  $\delta > 1.2$ . The extrema of  $C_v$ ,  $D_{1s}$  and  $D_{2s}$  clearly scale as  $\sim L^2$  when even smaller lattices are included into our analysis.

#### IV. DISCUSSION

It is interesting to compare the phase transitions in 3NN12 and 3NN1 models with those obtained in the 1NN model. This model has a critical line of the BKT-type phase transitions (frustrated structure) in between temperature points  $T_1$  and  $T_2$ . At  $T < T_1$  the AFM LRO phase is formed and at  $T > T_2$  the phase is paramagnetic<sup>36</sup>.

Both 3NN models also demonstrate the critical line of two BKT-type phase transitions. As in the 1NN model, the temperature range between these two points decreases with increase of a single-ion anisotropy parameter  $\delta$ , and these two BKT-type transitions flow into one first-order phase transition into the AFM LRO phase at some  $\delta_c$  (see phase diagram of all three models in Fig. 14 a, b and d). The  $\delta_c = 1.47^{36}$ , 1.3 and 1.2 for the 1NN, 3NN12 and 3NN1 models, respectively. The range at  $\delta > \delta_c$  is called the range III throughout this paper.

As might be seen in Fig. 14, from  $\delta = 0$  and up to  $\delta_c$  the phase transition temperature to the LRO AFM phase at  $T_1$  (low temperature end of the BKT-type phase transitions line) does not depend on the model.

Correspondingly, the transition properties of the 1NN and 3NN12 models at lower temperature are very similar in almost all interval of  $\delta$  values. At higher temperature and  $\delta < \delta_c$  these two models have notable differences: where the 1NN model demonstrates higher temperature paramagnetic-to-BKT-type phase transition at  $T_2$  and lower temperature transition at  $T_1$ , the 3NN12 model shows three transitions: (i) phase transition at  $T_c$  from paramagnetic phase to the structure, which has the stoichiometry and separate domains of the LRO AFM phase, (ii) higher-temperature transition to the BKT-type phase at  $T_2$  and (iii) lower temperature transition at  $T_1$ . The difference in magnitude of  $T_2$  occurs, because the 3NN12 model has higher entropy, i. e. larger number of free sites for hopping and higher probability of inhomogeneous distribution of particles into domains. Therefore the frus-

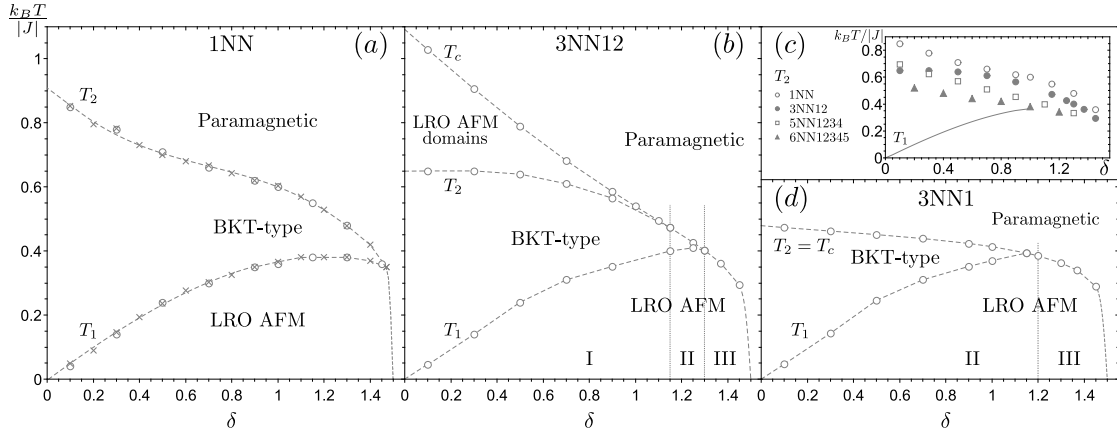


FIG. 14. (Color online) The phase diagrams of all three models: (a) 1NN ( $L = 48$ ), (b) 3NN12 ( $L = 180$ ) and (d) 3NN1 ( $L = 180$ ). (c) The dependence of transition temperature  $T_2$  on a chosen model with full exclusion (see text). The crosses in (a) are the results of Ref. <sup>36</sup>. Dashed lines are guides to the eye.

trated phase in the 3NN12 model disorders at lower temperature than in the 1NN model.

The occurrence of phase transition at  $T_c$  is related to the fact that exclusions make the energy and other thermodynamic functions more abrupt at higher temperature, i.e. exclusions create inhomogeneous distribution of particles in disordered phase. Thus, income of particles is hindered and their coverage  $c$  is artificially maintained too small for that particular temperature (in comparison to the 1NN model). Decrease of temperature enhances AFM correlations, and the “normal” coverage is recovered by sudden increase of  $c$ . This might be seen e.g. in  $c(T)$  dependences in Fig. 6 or temperature dependences of internal energy which result in sharp peaks of  $C_v$  at  $T_c$ . Thus, the “semi-ordered” AFM phase has a chance to form in the 3NN12 model at a bit higher temperature than the frustrated phase occurs. The hump in  $c(T)$  dependence marks the region of frustrated phase between  $T_1$  and  $T_2$ . In this temperature range the center sites of the hexagons (which are formed by alternating variables  $\pm 1$  on the vertices) are partially filled. Thus, in the 3NN12 model the preconditions (relatively low temperature and stoichiometry corresponding to the AFM phase) allows for the AFM domains-phase to occur just before the hump. Higher concentration and correspondingly broader hump (lower values of  $\delta$ ) shift the  $T_c$  value to higher temperature, while lower concentration ( $\delta > 1$ ) make the hump small and  $T_c \rightarrow T_2$ .

The entropy of the 3NN1 model (number of free sites for hopping) is even higher than that of the 1NN or 3NN12 model. Therefore the temperature of the phase transition from the paramagnetic phase for the 3NN1 model is the lowest of the three models. Moreover, due to relative entropy increase, this phase transition occurs at such a temperature which lies in temperature limits of the line of the the BKT-type critical points of the 1NN model. Therefore, contrary to the 1NN model, which has the line of critical BKT-type points between  $T_1$  and  $T_2$ ,

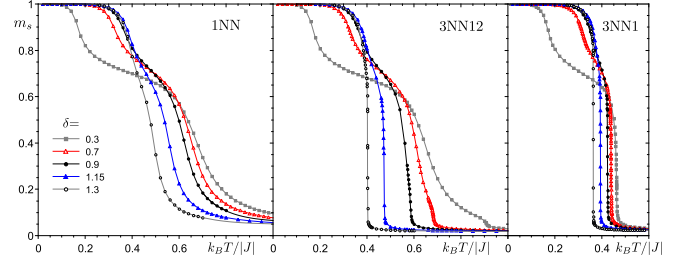


FIG. 15. (Color online) Temperature dependence of staggered magnetization for three models  $\delta = 0.3, 0.7, 0.9, 1.15$  and  $1.3$ . The results were obtained for lattice sizes  $L = 180$  (both 3NN models) and  $48$  (1NN model).

and the 3NN12 model, which (at least in part of  $\delta$  interval) demonstrates three phase transitions ( $T_1$ ,  $T_2$  and  $T_c$ ), the 3NN1 model shows reduced temperature interval of the BKT-type points line. The end point of this line at  $T_2$  coincides with  $T_c$  for all values of  $\delta$  and, as shown by our analysis, most likely, does not belong to the BKT-type phase transitions. Our analysis cannot distinguish, whether the two transitions merge into one point or they are separate transitions at extremely close temperatures with  $T_2 \lesssim T_c$ , a well-known situation for transitions to frustrated systems<sup>34,47</sup>. Note, that  $T_c$  and  $T_2$  for the 3NN12 model coincide only at narrow interval of  $1.15 < \delta < 1.3$  (compare abrupt behaviour of  $m_s(T)$  at this region of the 3NN12 model with that of the 3NN1 model in all interval of  $\delta$  values, see Fig. 15).

Analyzing the obtained energy histograms at  $T_c$  point, we found that the histograms are two-peaked in all interval of  $\delta$  values in both 3NN12 and 3NN1 models. However, the position of the saddle point in these histograms clearly depends on  $\delta$ . The  $\delta$ -dependences of interface tension, latent heat and Binder cumulants demonstrate that there are three ranges of behavior of phase transitions. In range III the transition at  $T_1 = T_2 = T_c$  is clearly

of the first order. This is evidenced by two-peaked histograms with a saddle point which is either very deep or decreasing with increase of  $L$ . The magnitudes of critical exponents  $\alpha/\nu$  and  $1/\nu$  are around 2. The histograms in intermediate range II ( $T_1 < T_2 = T_c$ ) have higher saddle point than those in region III, but it also decreases with increase of  $L$ . This allows to attribute the transition in this range to the first order, too. However, in this range the finite size scaling at the  $T_c$  point gives critical exponents different from (though rather close to) 2.

We could not present a definite answer about the type of the phase transition at  $T_c$  in region I of the 3NN12 model ( $T_1 < T_2 < T_c$ ). The histograms are two-peaked here, but the saddle point is rather high. Extrapolation of the values of interface tension and latent heat at lattice sizes used in this paper shows that they approach finite limits at  $L \rightarrow \infty$ . Rather controversial is the  $L$ -dependence of the order parameter which indicates that interpretation of the phase transition at  $T_c$  in terms of critical exponents might be inconsistent. This would allow to attribute this transition to a “weak” first-order phase transitions observed in some diluted and frustrated systems<sup>45</sup>. Nevertheless, we cannot completely rule out the possibility of a second-order phase transition manifesting itself as vanishing of the latent heat at much larger lattices than used here.

It should be noted that the 3NN12 model is a unique model in which the splitting of the higher temperature phase transition into two transitions, at  $T_c$  and  $T_2$ , occurs. In addition to this model, two other models with full exclusions up to interaction distance were also studied: the 5NN model with exclusions up to 4NN (5NN1234) and 6NN model with exclusions up to 5NN (6NN12345). All models except 3NN12 demonstrate one higher temperature phase transition at  $T_2 = T_c$ . The transition temperature at  $T_2$  and the parameter  $\delta_c$  in all models with full exclusions for entropic reasons gradually decreases with increase of interaction distance of the model (see Fig. 14c). For  $\delta < \delta_c$  the transition at  $T_2$  is the higher-temperature BKT-type phase transition for the 1NN (no  $T_c$ ) and 3NN12 ( $T_2 < T_c$ ) models, and of the first order for the 5NN1234 ( $T_2 = T_c$ ) and 6NN12345 ( $T_2 = T_c$ ) models.

Similar phase diagram as of the 3NN12 model might be observed in other frustrated systems. The phase transitions from paramagnetic to fully frustrated (FF) phase in square  $\phi^4$  FFX model<sup>47</sup> proceed either through (i) Ising and BKT phase transitions sequence with very close transition temperatures (at small values of parameter  $D$  similar to our  $\delta$ ), (ii) tricritical region (intermediate values of  $D$ ) featuring histograms with high saddle point or (iii) first order phase transitions (high values of  $D$ ).

Here we studied strongly diluted lattices with small concentration of particles (spins). Such studies require huge computer resources and therefore might leave some questions not completely answered. However, the main tendencies are quite clear: exclusions do not affect the low temperature phase transition; they make the high

temperature phase transition more abrupt; rescaling of lattice stimulate the entropic effects and decreases the high temperature phase transition temperature; in a case of the 3NN12 model the formation of domains of low-temperature structure might reveal itself as a phase transition at high temperature.

## V. ACKNOWLEDGEMENTS

We are grateful to Wolfhard Janke for reading of the manuscript and valuable discussions. A. Ibenskas acknowledges funding support by European Union Structural Funds project Postdoctoral Fellowship Implementation in Lithuania (VP1-3.1-ŠMM-01-V-02-004).

- <sup>1</sup>L. Bartels, *Nature Chemistry* **2**, 87 (2010).
- <sup>2</sup>J. V. Barth, *Annu. Rev. Phys. Chem.* **58**, 375 (2007).
- <sup>3</sup>A. Dmitriev, N. Lin, J. Weckesser, J.V. Barth, and K. Kern, *J. Phys. Chem. B* **106**, 6907 (2002).
- <sup>4</sup>Z. Li, B. Han, L.J. Wan, and Th. Wandlowski, *Langmuir* **21**, 6915 (2005).
- <sup>5</sup>Y. C. Ye, W. Sun, Y. F. Wang, X. Shao, X. G. Xu, F. Cheng, J. L. Li, and K. Wu, *J. Phys. Chem. C* **111**, 10138 (2007).
- <sup>6</sup>S. Griessl, M. Lackinger, M. Edelwirth, M. Hietschold, and W.M. Heckl, *Single Mol.* **3**, 25 (2002).
- <sup>7</sup>M. Lackinger, S. Griessl, W.M. Heckl, M. Hietschold, and G.W. Flynn, *Langmuir* **21**, 4984 (2005).
- <sup>8</sup>K.G. Nath, O. Ivasenko, J.M. MacLeod, J.A. Miwa, J.D. Wuest, A. Nanci, D.F. Perepichka, and F. Rosei, *J. Phys. Chem. C* **111**, 16996 (2007).
- <sup>9</sup>L. Kampschulte, T. L. Werblowsky, R. S. K. Kishore, M. Schmitt, W. M. Heckl, and M. Lackinger, *J. Am. Chem. Soc.* **130**, 8502 (2008).
- <sup>10</sup>R. Gutzler, T. Sirtl, J. F. Dienstmaier, K. Mahata, V. M. Heckl, M. Schmitt, and M. Lackinger, *J. Am. Chem. Soc.* **132**, 5084 (2010).
- <sup>11</sup>J. A. Theobald, N. S. Oxtoby, M. Phillips, N. R. Champness, P. H. Beton, *Nature* **424**, 424 (2003).
- <sup>12</sup>U. K. Weber, V. M. Burlakov, L. M. A. Perdigo, R. H. J. Fawcett, P. H. Beton, N. R. Champness, J. H. Jefferson, G. A. D. Briggs, and D. G. Pettifor, *Phys. Rev. Lett.* **100**, 156101 (2008).
- <sup>13</sup>F. Silly, U. K. Weber, A. Q. Shaw, V. M. Burlakov, M. R. Castell, G. A. D. Briggs, and D. G. Pettifor, *Phys. Rev. B*, **77**, 201408 (2008).
- <sup>14</sup>Y. Li, Z. Ma, G. Qi, Y. Yang, Q. Zeng, X. Fan, C. Wang, and W. Huang, *J. Phys. Chem. C* **112**, 8649 (2008).
- <sup>15</sup>G. Pawin, K. L. Wong, K.-Y. Kwon, and L. Bartels, *Science*, **313**, 961 (2006).
- <sup>16</sup>T. Misiūnas and E. E. Tornau, *J. Phys. Chem. B* **116**, 2472 (2012).
- <sup>17</sup>G. M. Bell and D. A. Lavis, *J. Phys. A: Gen. Phys.* **3**, 568 (1970).
- <sup>18</sup>C. E. Fiore, M. M. Szortyka, M. C. Barbosa, and V. B. Henriques, *J. Chem. Phys.* **131**, 164506 (2009).
- <sup>19</sup>M. Blume, *Phys. Rev.* **141**, 517 (1966); H. W. Capel, *Physica (Utr.)* **32**, 966 (1966).
- <sup>20</sup>G. D. Mahan and S. M. Girvin, *Phys. Rev. B* **17**, 4411 (1978).
- <sup>21</sup>M. Blume, V. J. Emery, and R. B. Griffiths, *Phys. Rev. A*, **4**, 1071 (1971); J. Sivardiere and J. Lajzerowicz, *Phys. Rev. A* **11**, 2090, 1975.
- <sup>22</sup>A. P. Young and D. A. Lavis, *J. Phys. A: Gen. Phys.* **12**, 229 (1979).
- <sup>23</sup>M. A. A. Barbosa and V. B. Henriques, *Phys. Rev. E* **77**, 051204 (2008).
- <sup>24</sup>R. M. F. Houtappel, *Physica (Utr.)* **16**, 425 (1950); G. H. Wannier, *Phys. Rev.* **79**, 357 (1950); R. J. Baxter, *J. Phys. A* **13**, L61 (1980).

- <sup>25</sup>A. Ibenskas and E. E. Tornau, Phys. Rev. E **86**, 051118 (2012).
- <sup>26</sup>V. Petrauskas, S. Lapinskas, and E. E. Tornau, J. Chem. Phys. **120**, 11815 (2004).
- <sup>27</sup>S. Fortuna, D. L. Cheung, and A. Troisi, J. Phys. Chem. B **114**, 1849 (2010).
- <sup>28</sup>M. Šimėnas, A. Ibenskas, and E. E. Tornau, Phase Transitions **86**, 866 (2013).
- <sup>29</sup>M. Šimėnas and E. E. Tornau, J. Chem. Phys. **139**, 154711 (2013).
- <sup>30</sup>M. Schick, J. S. Walker, and M. Wortis, Phys. Rev. B **16**, 2205 (1977); N. Berker, S. Ostlund, and F. A. Putnam, Phys. Rev. B **17**, 3650 (1978).
- <sup>31</sup>W. F. Wreszinski and S. R. A. Salinas, Disorder and competition in soluble lattice models, Series on advances in statistical mechanics, vol. 9, World Scientific, 1993.
- <sup>32</sup>S. Miyashita, Proc. Jpn. Acad., Ser. B **86**, 643 (2010); S. Miyashita, H. Kitatani, and Y. Kanada, J. Phys. Soc. Jpn **60**, 1523 (1991).
- <sup>33</sup>J. L. Cardy, J. Phys. A: Math. Gen. **13**, 1507 (1980) .
- <sup>34</sup>J. D. Noh, H. Rieger, M. Enderle, and K. Knorr, Phys. Rev. E **66**, 026111 (2002).
- <sup>35</sup>T. Surungan, Y. Okabe and Y. Tomita, J. Phys. A: Math. Gen. **37**, 4219 (2004).
- <sup>36</sup>M. Žukovič and A. Bobák, Phys. Rev. E **87**, 032121 (2013).
- <sup>37</sup>P. D. Coddington and L. Han, Phys. Rev. B **61**, 2635 (1994).
- <sup>38</sup>A. M. Ferrenberg and A. M. Swendsen, Phys. Rev. Lett. **61**, 2635 (1988); **63**, 1658 (1989).
- <sup>39</sup>A. M. Ferrenberg and D. Landau, Phys. Rev. B **44**, 5081 (1991).
- <sup>40</sup>M. S. S. Challa, D. P. Landau, and K. Binder, Phys. Rev. B **34**, 1841 (1986).
- <sup>41</sup>J.M. Kosterlitz and D.J. Thouless, J. Phys. C: Solid State Phys. **6**, 1181 (1973).
- <sup>42</sup>M. S. S. Challa and D. P. Landau, Phys. Rev. B **33**, 437 (1986).
- <sup>43</sup>J.V. José, L.P. Kadanoff, S. Kirkpatrick, and D.R. Nelson, Phys. Rev. B **16**, 1217 (1977).
- <sup>44</sup>D. P. Landau, Phys. Rev. B **27**, 5604 (1983).
- <sup>45</sup>C. Chatelain, P.-E. Berche, B. Berche, and W. Janke, Comp. Phys. Comm. **147**, 431 (2002); S. Jin, A. Sen, W. Guo, and A. W. Sandvik, Phys. Rev. B **87**, 144406 (2013); A. Kalz and A. Honecker, Phys. Rev. B **86**, 134410 (2012).
- <sup>46</sup>M. P. M. den Nijs, J. Phys. A **12**, 1857 (1979); B. Nienhuis, A. N. Berker, E. K. Riedel, and M. Schick, Phys. Rev. Lett. **43**, 737 (1979); B. Nienhuis, J. Phys. A **15**, 199 (1982).
- <sup>47</sup>M. Hasenbusch, A. Pelissetto, and E. Vicari, J. Stat. Mech. **P12002**, 1 (2005); Phys. Rev. B **72**, 184502 (2005).